KSCE Journal of Civil Engineering (2016) 20(4):1501-1513

DOI 10.1007/s12205-015-0271-x

Structural Engineering

pISSN 1226-7988, eISSN 1976-3808
www.springer.com/12205

Coupled Flutter Analysis of Long-span Bridges Using Full Set of Flutter Derivatives

Tan-Van Vu*, Young-Min Kim, and Hak-Eun Lee*****

Received April 6, 2015/Accepted July 3, 2015/Published Online August 21, 2015

Abstract

A convenient and effective finite element-based method for coupled flutter analysis of long-span bridges is presented. The exact formulation of the aerodynamic self-excited forces with eighteen flutter derivatives utilized by complex notation is proposed. The predictions of the flutter wind speed and the critical frequency are compared with those either given by existing methods or the wind tunnel test showing the effectiveness and accuracy of the present approach. Numerical flutter analysis for an asymmetric bridge is the application for engineering practice, and its obtained results highlight the important role of the first lateral bending and torsional mode in generating the coupled flutter. Multi-mode analyses that are based on only the symmetrical modes can predict accurately the bridge flutter onset. The consistent self-excited aerodynamic force formulations produce the flutter velocity that is closer to the experimental one of full-bridge model in the wind tunnel.

Keywords: *long-span bridges, coupled flutter, direct analysis, multi-mode analysis, complex eigenvalue analysis, state space method*

1. Introduction

Due to their large flexibility, large-scale, low structural damping structure and slenderness, long-span cable-supported bridges are highly susceptible to a variety of wind-induced vibrations. In this regard, the interaction between the wind load and the bridge can cause several undesirable aerodynamic phenomena including vortex shedding, galloping, buffeting and flutter. Among them, the flutter instability is the most dangerous factor as it can cause divergent oscillations, which leads to the damage of structures. For instance, as the case of the Old Tacoma Narrows Bridge that was failed shortly after its completion in 1940. Flutter phenomena of a long-span bridge occurs whenever the accumulated energy generated by the approaching wind flow is larger than the internal energy dissipated by structural damping. Flutter analysis aims to predict the lowest critical wind velocity corresponding to the flutter frequency that induces the aeroelastic instability. As a regulation in the design stage of long-span bridges, the critical flutter wind velocity of a bridge must exceed the meteorological possible wind velocities at the bridge site.

Since the collapse of the Old Tacoma Narrows Bridge, considerable research has been made to develop methods for analyzing the instability aerodynamics problems of long-span bridges. A traditional approach is based on fundamental vertical bending and torsional modes of bridge vibration to solve the coupled flutter problem. As one of the pioneers in this research area, Bleich (1949) analyzed this problem by applying Theodorsen's airfoil theory to evaluate the unsteady aerodynamic forces on thin–airfoil cross sections. This approach can be extended to calculate the flutter onset for long-span bridges with streamlined sections, but the problems of overestimated values for decks with bluff sections may be its disadvantages.

In 1971, Scanlan and Tomko (1971) proposed the flutter derivatives concept that allows the aerodynamics forces acting on real bridge decks to be represented based on data measured from section model tests. Relying on the pioneered works, various methods based on the bimodal approach were proposed to analyze the flutter bridge problem. The evolution of the approach can be traced by referring to the works of Scanlan (1978); Simiu and Scanlan (1996); Matsumoto (1999); Chen and Kareem (2006, 2007); Bartoli and Mannini (2008); Lee *et al.* (2011); Vu *et al.* (2011a, 2013). Nevertheless, such approaches may fail to include the worst scenario (Namini *et al.*, 1992) or lead to extremely conservative results in certain cases, when the mode shapes of the torsional and vertical vibration of the prototype differ strongly; hence these approximated approaches are often used at the preliminary design stage.

A more accurate flutter prediction should then be based on spatial modeling such as full model tests or spatial aeroelastic analysis. Determination of the onset flutter by using the spatial analysis including the finite element model and the flutter derivatives concept proves particularly efficient. Within this framework, flutter analysis approaches can be grouped into two

*Ph.D., Dept. of Civil Engineering, HoChiMinh City University of Architecture, Vietnam (Corresponding Author, E-mail: van.vutan@uah.edu.vn)
**Member, Ph.D., Institute of Construction Technology, DAEWOO E&C Co., Ltd., Suwon 440-800, Korea (E-mail: ymkim@dwconst.co.kr)
***Member, Professor, School of Civil, Environmental and Architectural Engineering, Korea University, Seoul 136-701 Korea (E-mail: helee@korea.ac.kr)

broad categories as follows: (i) the direct approach where the instability flutter analysis is applied directly to the full three-dimensional finite element model of the bridge structures (Dung *et al.*, 1998; Starossek, 1998; Ge and Tanaka, 2000; Ding *et al.*, 2002); and (ii) the multi-mode approach, which is based on the fact that the flutter responses of long-span bridges are predicted using a modal superposition technique consisting of several low-frequency natural modes of bridge structures (Agar, 1989; Namini *et al.*, 1992; Tanaka *et al.*, 1992; Jain *et al*., 1996; Katsuchi *et al.*, 1999; Chen *et al*., 2000; Ding *et al.*, 2002; Zhang *et al.*, 2002; Zhang and Brownjohn, 2005; Mishra *et al.*, 2008).

Most numerical methods on bridge flutter that describe the aerodynamics forces with real numbers are as proposed by the pioneering researchers (Agar, 1989; Namini *et al.*, 1992; Tanaka *et al.*, 1992; Dung *et al.*, 1998; Ge and Tanaka, 2000; Zhang *et al.*, 2002; Jain *et al*., 1996; Chen *et al*., 2000). However, some studies (Agar, 1989; Namini *et al.*, 1992; Tanaka *et al.*, 1992; Dung *et al.*, 1998; Ge and Tanaka, 2000; Zhang *et al.*, 2002) have neglected the role of Lateral Flutter Derivatives (LFDs), while others (Jain *et al*., 1996; Chen *et al*., 2000) have utilized the LFDs based upon the quasi-steady theory. Nevertheless, the role of the individual LFDs in the flutter phenomenon was investigated by other scientists. Katsuchi *et al.* (1999) reported that the LFDs P_i^* (i = 2,3,5,6), extracted from the wind tunnel test, played a significant and destabilizing role in the flutter onset of the Akashi-Kaikyo Bridge. It also has been observed, for instance by Zhang and Brownjohn (2005), that all $P_i^*(i = \overline{1,6})$-related utter derivatives have a stabilizing effect on the utter onset. On the other hand, Mishra *et al.* (2008) highlighted the role of each LFDs in the utter phenomenon, it is necessary to investigate the problem of aerodynamic instability of the long and super-long span bridges by using the full set of experimental flutter derivatives of $A_i^*, H_i^*, P_i^*(i = \overline{1,6})$. It is because the interaction amongst the self-excited forces in the vertical, lateral and torsional directions can generate coupled flutter of these bridges and the exclusion LFDs leads to overestimation of the flutter wind velocity.

The main objective of the present contribution is to present a convenient and effective finite element-based method for coupled flutter analysis of long-span cable-supported bridges. The present analysis is essentially based on the existing framework of complex notation (Starossek, 1998; Ding *et al.*, 2002). However, the proposed approach differs from the previous works in the fact that all 18 experimental flutter derivatives are employed for deriving the consistent forms of the aerodynamic self-excited forces. In addition, a linearization technique is proposed to convert the flutter equation of the bridge into the generalized eigenvalue problem. Comparative studies and the coupled flutter analysis of the asymmetric bridge with a main span of 510 m are additionally investigated to illustrate the effectiveness of the proposed approach. The role of the first lateral bending and torsional mode for generating the coupled flutter and the accurate prediction onset flutter of the asymmetric cable-stayed long-span bridge is highlighted.

2. Aerodynamic Force Model

2.1 Uniformly Distributed Forces

The self-excited forces per unit span of a bridge deck, arising from the interaction between the smooth wind flow and the bridge, that include the lift force L_{ae}, drag force D_{ae} and pitching moment M_{ae}, can be expressed as a linear combination of nodal displacement and velocity. The entire complement of 18 flutter derivatives are given by (Sarkar *et al.*, 1994; Jain *et al.*, 1996):

$$L_{ae} = \frac{1}{2}\rho U^2 B\left[KH_1^*\frac{\dot{h}}{U} + KH_2^*\frac{B\dot{\alpha}}{U} + K^2H_3^*\alpha + K^2H_4^*\frac{h}{B} + KH_5^*\frac{\dot{p}}{U} + K^2H_6^*\frac{p}{B}\right] \tag{1a}$$

$$D_{ae} = \frac{1}{2}\rho U^2 B\left[KP_1^*\frac{\dot{p}}{U} + KP_2^*\frac{B\dot{\alpha}}{U} + K^2P_3^*\alpha + K^2P_4^*\frac{p}{B} + KP_5^*\frac{\dot{h}}{U} + K^2P_6^*\frac{h}{B}\right] \tag{1b}$$

$$M_{ae} = \frac{1}{2}\rho U^2 B^2\left[KA_1^*\frac{\dot{h}}{U} + KA_2^*\frac{B\dot{\alpha}}{U} + K^2A_3^*\alpha + K^2A_4^*\frac{h}{B} + KA_5^*\frac{\dot{p}}{U} + K^2A_6^*\frac{p}{B}\right] \tag{1c}$$

where $A_i^*, H_i^*, P_i^*(i = \overline{1,6})$ are the non-dimensional flutter derivatives dependent upon the reduced frequency, $K(=B\omega/U)$, ρ is the air mass density, U is the mean wind velocity, $B = 2b$ is the bridge deck width, and ω is the circular frequency. h, p and α are the vertical, lateral and torsional displacement, respectively. The dot in the equations indicates the differentiation with respect to time. The motion-dependent aeroelastic forces and the heave, sway and torsional deformations are shown their positive directions in Fig. 1.

Equation (1) represents the real-number expressions for the aeroelastic forces, the corresponding complex-number expressions of the self-excited forces can be expressed in the extended format below

$$L_{ae} = \omega^2\pi\rho b^2(C_{Lh}h + C_{Lp}p + bC_{L\alpha}\alpha) \tag{2a}$$

$$D_{ae} = \omega^2\pi\rho b^2(C_{Dh}h + C_{Dp}p + bC_{D\alpha}\alpha) \tag{2b}$$

$$M_{ae} = \omega^2\pi\rho b^2(bC_{Mh}h + C_{Mp}p + b^2C_{M\alpha}\alpha) \tag{2c}$$

where $C_{rs}(r = D, L, M; s = h, p, \alpha)$ are the complex coefficients of self-excited forces. By comparing the aerodynamic force

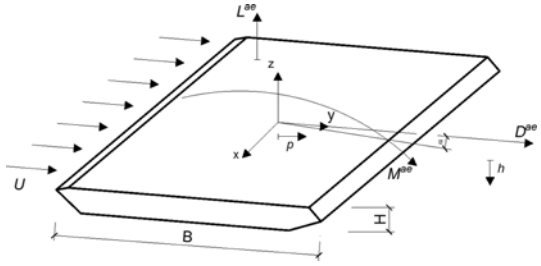

Fig. 1. Sign Convention of Aerodynamic Forces and Deformations for a Bridge Deck

expressions in real and complex notation, these coefficients can be found as,

$$C_{Lh} = \frac{2}{\pi}(H_4^* + iH_1^*),\ C_{Lp} = \frac{2}{\pi}(H_6^* + iH_5^*),\ C_{L\alpha} = \frac{4}{\pi}(H_3^* + iH_2^*) \quad (3a)$$

$$C_{Dh} = \frac{2}{\pi}(P_6^* + iP_5^*),\ C_{Dp} = \frac{2}{\pi}(P_4^* + iP_1^*),\ C_{D\alpha} = \frac{4}{\pi}(P_3^* + iP_2^*) \quad (3b)$$

$$C_{Mh} = \frac{4}{\pi}(A_4^* + iA_1^*),\ C_{Mp} = \frac{4}{\pi}(A_6^* + iA_5^*),\ C_{M\alpha} = \frac{8}{\pi}(A_3^* + iA_2^*) \quad (3c)$$

2.2 Consistent Aerodynamic Matrix Formulation

Figure 2 shows a three-dimensional space frame element oriented in its local axes. This element has 12 degrees-of-freedom, $q_i (i = \overline{1,12})$, which are detailed as follows: two axial displacements along the X_e-axis (q_1 and q_7), two flexural displacements along the Y_e-axis (q_2 and q_8), two flexural displacements along the Z_e-axis (q_3 and q_9), two torsional rotations around the X_e-axis (q_4 and q_{10}), two flexural rotations around the Y_e-axis (q_5 and q_{11}), and two flexural rotations around the Z_e-axis (q_6 and q_{12}). In the framework of the classical finite element method, the dynamic axial $u(x, t)$ and the torsional $\alpha(x, t)$ response are respectively approximated by

$$u(x,t) = \{N_1(x)\}^T\{q_u(t)\}_e,\ \alpha(x,t) = \{N_1(x)\}^T\{q_\alpha(t)\}_e \quad (4a,4b)$$

where $\{N_1(x)\}^T = \{1 - x/L,\ x/L\}$ is a vector of linear spatial shape function, and $\{q_u(t)\}_e^T = \{q_u(t),\ q_7(t)\}$ and $\{q_\alpha(t)\}_e^T = \{q_4(t),\ q_{10}(t)\}$ represent the vector of axial and torsional displacements, respectively. The superscript T indicates a vector transpose while L indicates the element length. Also, the dynamic vertical and lateral response are approximated respectively as follows:

$$h(x,t) = \{N_2(x)\}^T\{q_h(t)\}_e,\ p(x,t) = \{N_2(x)\}^T\{q_p(t)\}_e \quad (5a,5b)$$

where $\{N_2(x)\}^T = \left\{\begin{matrix} 1-3(x/L)^2 + 2(x/L)^3,\ 3(x/L)^2 - 2(x/L)^3, \\ x - 2L(x/L)^2 + L(x/L)^3,\ -L(x/L)^2 + L(x/L)^3 \end{matrix}\right\}$

is a vector of the cubic spatial shape function, and the vector of the vertical and lateral displacements are defined as $\{q_h(t)\}_e^T = \{q_2(t),\ q_8(t),\ q_6(t),\ q_{12}(t)\}$ and $\{q_p(t)\}_e^T = \{q_3(t),\ q_9(t),\ q_5(t),\ q_{11}(t)\}$, respectively.

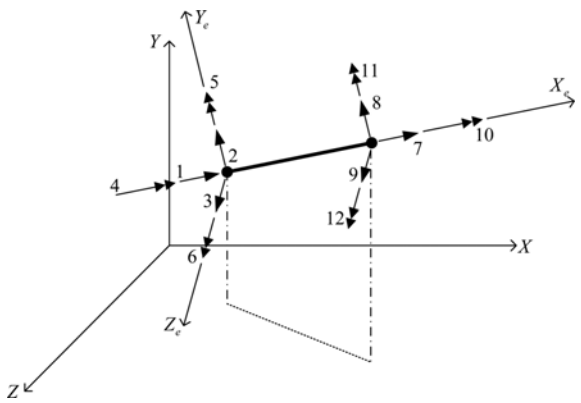

Fig. 2. Sign Convention for the 12-degree-of-freedom Space Beam Element

For a three-dimensional Bernoulli-Euler beam, the aerodynamic forces corresponding to a vector of nodal forces can be related to the nodal displacement vector by a linear matrix operation. Because it is assumed that the flow in each cross-section remains unaffected by the flow in adjoining sections, and the variation of the external work acting on the element produced by the self-exited forces is expressed as

$$\delta W_{ae} = \int_0^L L_{ae}\delta h(x,t)dx + \int_0^L L_{ae}\delta p(x,t)dx + \int_0^L M_{ae}\delta\alpha(x,t)dx \quad (6)$$

$$\delta W_{ae} = \omega^2 \begin{bmatrix} \pi\rho b^2 \int_0^L [C_{Lh}h(x,t) + C_{Lp}p(x,t) + bC_{L\alpha}\alpha(x,t)]\delta h(x,t)dx + \\ \pi\rho b^2 \int_0^L [C_{Dh}h(x,t) + C_{Dp}p(x,t) + bC_{D\alpha}\alpha(x,t)]\delta p(x,t)dx + \\ \pi\rho b^2 \int_0^L [C_{Mh}h(x,t) + C_{Mp}p(x,t) + b^2C_{M\alpha}\alpha(x,t)]\delta\alpha(x,t)dx \end{bmatrix} \quad (7)$$

Substituting expressions (4) and (5) into Eq. (7), the external work due to the self-exited forces can be expressed as,

$$\delta W_{ae} = \omega^2 \int_0^L \left(\begin{bmatrix} \{\delta q_h(t)\}_e^T \pi\rho b^2 \begin{bmatrix} C_{Lh}\{N_2(x)\}\{N_2(x)\}^T\{q_h(t)\}_e + \\ C_{Lp}\{N_2(x)\}\{N_2(x)\}^T\{q_p(t)\}_e + \\ bC_{L\alpha}\{N_2(x)\}\{N_1(x)\}^T\{q_\alpha(t)\}_e \end{bmatrix} + \\ \{\delta q_p(t)\}_e^T \pi\rho b^2 \begin{bmatrix} C_{Dh}\{N_2(x)\}\{N_2(x)\}^T\{q_h(t)\}_e + \\ C_{Dp}\{N_2(x)\}\{N_2(x)\}^T\{q_p(t)\}_e + \\ bC_{D\alpha}\{N_2(x)\}\{N_1(x)\}^T\{q_\alpha(t)\}_e \end{bmatrix} + \\ \{\delta q_\alpha(t)\}_e^T \pi\rho b^2 \begin{bmatrix} bC_{Mh}\{N_1(x)\}\{N_2(x)\}^T\{q_h(t)\}_e + \\ bC_{Mp}\{N_1(x)\}\{N_2(x)\}^T\{q_p(t)\}_e + \\ b^2C_{M\alpha}\{N_1(x)\}\{N_1(x)\}^T\{q_\alpha(t)\}_e \end{bmatrix} + \end{bmatrix} dx \quad (8)$$

or

$$\delta W_{ae} = \omega^2\{\delta q(t)\}_e^T[A_{ae}^e]\{q(t)\}_e \quad (9)$$

where $[A_{ae}^e]$ is a so-called aerodynamic matrix, of which the elements derived from Eq. (8) are listed in the Appendix.

3. Equation of Motion-Analysis Methods

To obtain the discrete equations from the equation of motion for an element assemblage, one may utilize the Hamilton's principle:

$$\int_{t_1}^{t_2} (\delta T - \delta V + \delta W_d + \delta W_{ae})dt = 0 \quad (10)$$

where δT, δV and δW_d are the variation of the kinetic energy, the strain energy and the damping forces. They are well described in a number of finite-element textbooks. Accordingly, these variations can be expressed as (Weaver and Johnston, 1987)

$$\delta T = -\{\delta q(t)\}^T[M^e]\{\ddot{q}(t)\} \quad (11a)$$

$$\delta V = \{\delta q(t)\}_e^T[K^e]\{q(t)\}_e \quad (11b)$$

$$\delta W_d = -\{\delta q(t)\}_e^T[C^e]\{\dot{q}(t)\}_e \quad (11c)$$

where $[M^e]$, $[K^e]$ and $[C^e]$ are the square matrices of order 12, and also referred to as the mass, stiffness and damping matrices of the element, respectively. Substituting Eqs. (9) and (11) into Eq. (10), we have

$$\int_{t_1}^{t_2} \begin{pmatrix} -\{\delta q(t)\}_e^T[M^e]\{\ddot{q}(t)\}_e - \{\delta q(t)\}_e^T[K^e]\{q(t)\}_e - \\ \{\delta q(t)\}_e^T[C^e]\{\dot{q}(t)\}_e + \omega^2\{\delta q(t)\}_e^T[A_{ae}^e]\{q(t)\}_e \end{pmatrix} dt = 0 \quad (12)$$

This is because the Lagrangian function of an assemblage can be obtained by adding the energy contributions of the individual elements for the bridge structure. Thus, by adding and transforming all the matrices onto the global axes, the assembled equilibrium equations can be obtained as follows,

$$[M]\{\ddot{q}(t)\} + [C]\{\dot{q}(t)\} + [K]\{q(t)\} = \omega^2[A_{ae}]\{q(t)\} \quad (13)$$

Equation (13) represents the mathematical model of the structural system under the effect of wind load, wherein $[M]$, $[C]$, $[K]$ and $[A_{ae}]$ are the structural mass, damping, stiffness and aerodynamic matrices, respectively, and $\ddot{q}(t)$, $\dot{q}(t)$, $q(t)$ denote the structural displacement, velocity and acceleration vectors, respectively. It is noted that the damping matrix $[C]$ in the Eq. (13) is assumed to be of the Rayleigh type, in that it can be computed as a linear combination of the mass and stiffness matrices of the structure (Clough and Penzien, 1993).

3.1 Direct Flutter Analysis

Equation (13) is a system of the n-second-order differential equation with damping property (n is total number of dynamical degrees of freedom of the system). Using the exponential solution function $\{q(t)\} = \{\Delta\}e^{i\omega t}$, and substituting this into Eq. (13), the flutter equation can be obtained as follows:

$$\{(i\omega)^2([M]+[A_{ae}]) + i\omega[C] + [K]\}\{\Delta\}e^{i\omega t} = \{0\} \quad (14)$$

It is noted that the basic equation system of structural dynamics, being different with the real-number expression of the self-excited forces approach in additional term of $[A_{ae}]$ that is to be added to the mass matrix $[M]$. Since Eq. (14) does not contain any terms in U and thus it is to be solved for only two eigenvalues, ω and K. Accordingly, the solution as described by the present approach does not require a rather intricate multilevel iteration procedure.

Equation (14) can be rewritten in the form of $2n$-equations as follows:

$$\left(\begin{bmatrix} [C] & [K] \\ [I] & [0] \end{bmatrix} \begin{Bmatrix} i\omega\{\Delta\} \\ \{\Delta\} \end{Bmatrix} + (i\omega) \begin{bmatrix} ([M]+[A_{ae}]) & [0] \\ [0] & -[I] \end{bmatrix} \begin{Bmatrix} i\omega\{\Delta\} \\ \{\Delta\} \end{Bmatrix} \right) e^{i\omega t} = \begin{Bmatrix} \{0\} \\ \{0\} \end{Bmatrix} \quad (15)$$

where $[I]$ is the $n \times n$ identity matrix, $[0]$ is the $n \times n$ null matrix, and for a nontrivial solution to exist, the analysis of complex eigenvalues and eigenvectors of the system is converted into the following Generalized Eigenvalue Problem (GEP) with $2n$-eigenvalues and eigenvectors:

$$[P]\{Z\} = \lambda[Q]\{Z\} \quad (16)$$

where

$$[P] = \begin{bmatrix} [C] & [K] \\ [I] & [0] \end{bmatrix},\ [Q] = \begin{bmatrix} -[M]-[A_{ae}] & [0] \\ [0] & [I] \end{bmatrix},\ \{Z\} = \begin{Bmatrix} \lambda\Delta \\ \Delta \end{Bmatrix},\ \lambda = i\omega \quad (17a,b,c,d)$$

Equation (16) depends on the reduced frequency, K and vibration frequency, ω. With this equation, a complex eigenvalue analysis process can be employed to determine the eigenvalues of the structural system as follows. When K is fixed, solving Eq. (16) yields conjugate pairs of complex eigenvalues, i.e., $\lambda_j = \sigma_j \pm i\omega_j$ $(j = \overline{1,n})$ and the conjugate pairs of complex eigenvectors, i.e., $Z_j = r_j \pm is_j$ $(j = \overline{1,n})$ are obtained.

In the border case of onset flutter instability, the corresponding imaginary part of the complex eigenvalue λ_f has a zero real part, and a positive imaginary part. Hence, K must be fixed repeatedly until this condition is met. The critical wind speed, $U_f = B\omega_f/K$, wherein ω_f is the flutter frequency. For the purpose of practical flutter prediction, the lowest possible wind speed resulting in the aeroelastic instability is most important factor and of concern. The algorithmic implementation for the full order analysis is outlined in the following steps:

(1) Compute the reduced frequency, K_j from within the range of $[0, K_{max}]$ and a reduced frequency increment ΔK: $K_j = K_{j-1} + (j-1)\Delta K$

(2) Compute the flutter derivatives $A_i^{*(j)}$, $H_i^{*(j)}$, $P_i^{*(j)}(i = \overline{1,6})$ by the B-Spline interpolation technique, then construct the aerodynamic matrix, $[\mathbf{A}_{ae}^{(j)}]$

(3) Compute $\{\lambda_j\}_{1\times n} = \{\mu_j + i\omega_j\}_{1\times n}$ from solving the GEP defined by Eq. (16);

(4) Loop over the r^{th} complex modes $(r = \overline{1,n})$
If $[\mu_{j-1}^{(r)} \times \mu_j^{(r)}] \le 0$ or $\left|\mu_j^{(r)}\right| \le \varepsilon$, with $\varepsilon = 10^{-5}$ then,
- Compute the reduced frequency, $K_j^{f,(r)}$, and compute $\omega_j^{f,(r)}$ using the linear interpolation technique:

$$K_j^{f,(r)} = \frac{\mu_j^{(r)}K_{j-1} - \mu_{j-1}^{(r)}K_j}{\mu_j^{(r)} - \mu_{j-1}^{(r)}},\ \omega_j^{f,(r)} = \frac{\mu_j^{(r)}\omega_{j-1}^{(r)} - \mu_{j-1}^{(r)}\omega_j^{(r)}}{\mu_j^{(r)} - \mu_{j-1}^{(r)}}$$

- Compute

(5) Set $j = j + 1$:
If $K_j = K_{max}$, go to Step (6), otherwise repeat Step (1) to Step (4)

(6) Compute the lowest onset flutter for each complex mode r^{th}: $U_r^{f,\min} = \min_j\{U_j^{f,(r)}\}$ and $\omega_r^{f,\min} = \min_j\{\omega_j^{f,(r)}\}$ with $(j = \overline{1,n})$.

(7) Compute the lowest critical speed flutter; $U_f = \min\{U_r^{f,\min}\}$ and the flutter frequency $\omega_f = \min\{\omega_r^{f,\min}\}$ for all complex modes.

3.2 Multi-mode Flutter Analysis

For a linear elastic structure, wherein the structure system is a very large value of degrees- of- freedoms, the commonly used modal superposition technique is employed for solving the equation of motion by using the first m-structural natural modes $(m << n)$. Accordingly, the response in the displacement vector $\{q(t)\}$ can be approximated by

$$\{q(t)\} = [\Phi]\{y(t)\} \quad (18)$$

where $[\Phi]$ is the matrix of size $m \times n$ consisting of the mass-normalized mode shapes of selected m participating modes, and $\{y(t)\}$ denotes the mth-order vector of the generalized modal coordinate. Substituting Eq. (18) into Eq. (13), pre-multiplying $[\Phi]^T$, and then applying the orthogonal condition give the representing modal-motion equations as

$$[I]\{\ddot{y}\} + [\hat{C}]\{\dot{y}\} + ([\hat{K}] - \omega^2[A_{ae}])\{y\} = \{0\} \quad (19)$$

where $[\hat{C}] = [\Phi]^T[C][\Phi] = diag(2\omega_1\xi_1, 2\omega_2\xi_2, ..., 2\omega_m\xi_m)$ represents the generalized Rayleigh damping matrix [26], $[\Lambda] = [\Phi]^T[K][\Phi] = diag\ (\omega_1^2, \omega_2^2, ..., \omega_m^2)$ denotes the diagonal matrix of eigenvalues, and $[A_{ae}] = [\Phi]^T[A_{ae}][\Phi]$ indicates a generalized aerodynamic matrix.

Let the solution to Eq. (19) have the form $\{y(t)\} = \{\Delta^*\}e^{i\omega t}$, then the dimension of the GEP that is defined by Eq. (16) reduces to 2 m, namely

$$[P^*]\{Z^*\} = \lambda[Q^*]\{Z^*\} \quad (20)$$

where

$$[P^*] = \begin{bmatrix} [\hat{C}]\ [\Lambda] \\ [I^*]\ [0^*] \end{bmatrix},\ [Q^*] = \begin{bmatrix} -[I^*] - [\hat{A}_{ae}]\ [0^*] \\ [0^*] \qquad [I^*] \end{bmatrix},\ \{Z\} = \begin{Bmatrix} \lambda\Delta^* \\ \Delta^* \end{Bmatrix} \quad (21a,b,c)$$

with $[I^*]$ and $[0^*]$ are the $m \times m$ identity and null matrix, respectively.

4. Numerical Examples

The accuracy and computational efficiency of the new procedures are demonstrated by considering three illustrative examples. These examples include a cantilevered thin airfoil, a three-span cable-stayed bridge, and the asymmetric bridge. The first two examples are chosen to verify the accuracy of the proposed method wherein the aerodynamic forces matrix is calculated by using theoretical flutter derivatives. The third, the more complex example of engineering application of a cable-stayed bridge is selected primarily to determine the efficiency of the proposed multi-mode flutter analysis algorithm. The numerical results computed by the proposed methods are compared with previously published data. The formulation described above has been programmed by a FORTRAN 90 computer program named KDCWE (Vu, 2010). This program is also written to permit a user to define the structure's geometry and the flutter derivatives for deck section, if requested, the initial profile can be computed.

4.1 Flutter Analysis using Theoretical Flutter Derivative

The self-excited aerodynamic lift and moment acting on an idealized thin-airfoil cross section in smooth flow were first analytically calculated by Theodorsen, and flutter derivatives of A_i^*, $H_i^*(i = \overline{1,4})$ can be determined by the well-known circulation function (Theodorsen, 1935). Fig. 3 shows the evolution of the theoretical flutter derivatives with respect to the reduced wind speed. In this section, two typical examples are provided for the flutter analyses. The applications considered are that of a cantilevered thin airfoil and a three spans cable-stayed bridge

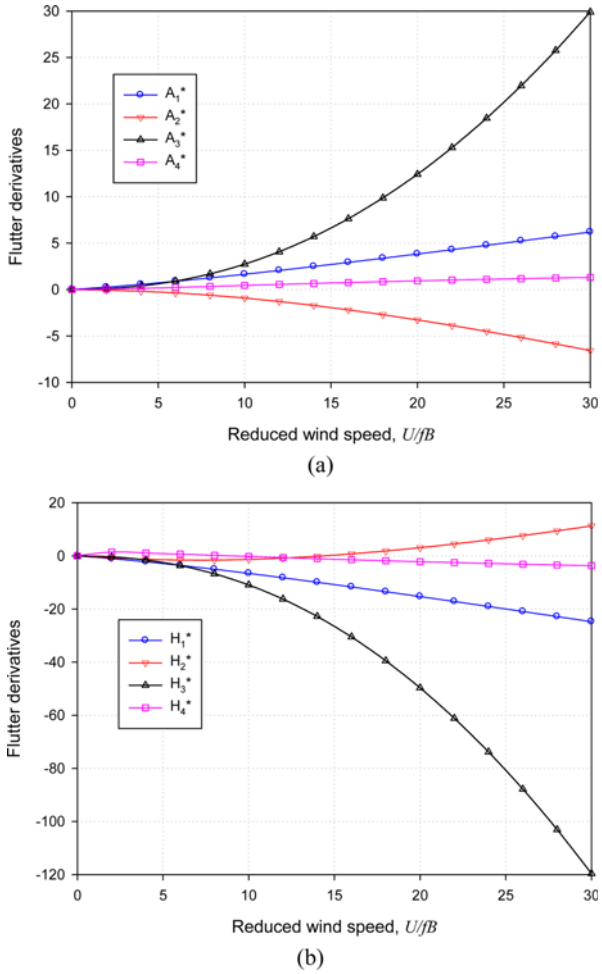

Fig. 3. Flutter Derivatives for the Thin Airfoil: (a) $A_i^*(i = 1, 2, 3, 4)$, (b) $H_i^*(i = 1, 2, 3, 4)$

structure, since their theoretical solutions of onset flutter are available.

4.1.1 Cantilevered Thin Airfoil

This problem was first considered by Ge and Tanaka (2000), where the cantilevered thin airfoil structure has a theoretical expression for the aerodynamic forces. This structure is simply modeled by eight space beam elements and has the main structural properties as follows: span $L = 200$ m; width $B = 40$ m; bending stiffness $EI_y = 1.8 \times 10^7$ MPa m^4, $EI_z = 2.1 \times 10^6$ MPa m^4; torsional stiffness $GJ_x = 4.1 \times 10^5$ MPa m^4; mass per unit length $m = 2 \times 10^4$ kg/m; mass moment of inertia per unit length $I_m = 5.44 \times 10^5$ kgm^2/m, and air mass density $\rho = 1.25$ kg/m^3. The zero damping is assumed for each natural mode of the structure. Firstly, the program uses the method (Arnoldi, 1951) from the ARPACK library program to perform a natural frequency analysis yielding the first seven eigen-modes result as gathered in Table 1. According to the computational steps described in the previous section, a complex eigenvalue analysis is employed for the wind-structure system.

In order to illustrate the pre-flutter and post-flutter behavior of

Table 1. Natural Frequencies and Mode Shape of the Cantilevered Thin Airfoil

Mode	Mode shape	Natural frequency, $\omega(rad/s)$		Error $\Delta\omega(\%)$
		Ge and Tanaka (2000)	Present	
1	V-1	0.888	0.901	1.4
2	T-1	2.152	2.160	0.4
3	V-2	5.473	5.645	3.1
4	T-2	6.372	6.562	3.0
5	L-1	8.314	8.390	0.9
6	T-3	10.350	10.717	3.5
7	T-4	13.930	14.121	1.4

Note: V = vertical; T = torsional; L = lateral

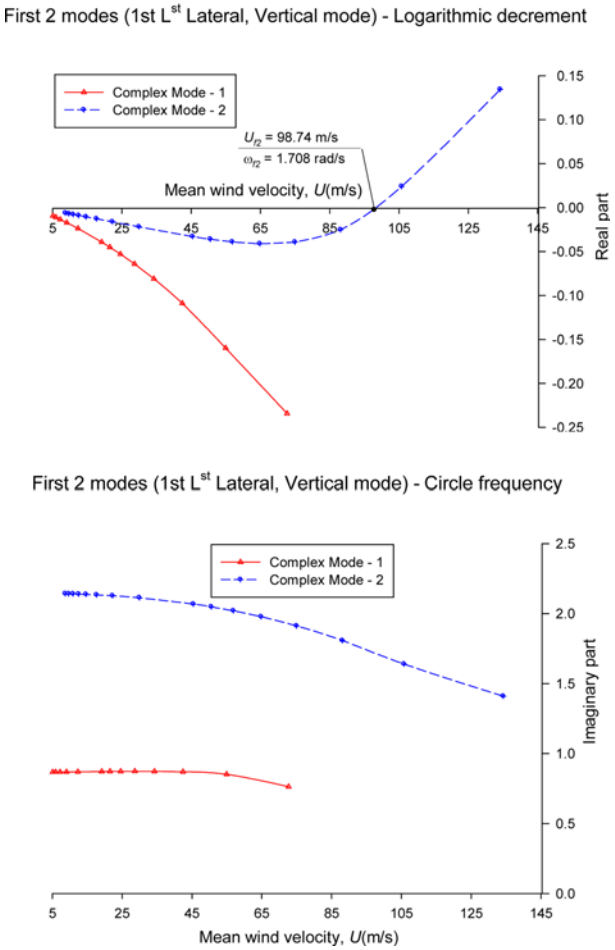

Fig. 4. Flutter Eigenvalue Evolution of the Cantilevered Structure Using First Two Modes

the cantilevered structure, a diagram illustrates the real part (logarithmic decrement σ_j) and imaginary part (oscillation frequency ω_j) versus the mean wind velocity corresponding to the range of the reduced frequency K_j as shown in Fig. 4 for the case of the multi-mode flutter analysis, which is based on the first two modes of this structure. The critical condition of the flutter instability is wherein an eigenvalue that is characterized by the real part passes to the zero point from the negative to the positive part, and the imaginary part becomes the corresponding frequency.

Table 2. Multi-mode Flutter Analysis Results of the Cantilevered Thin Airfoil

Modes Combined	Ge and Tanaka (2000)		Present		Error $\Delta U_f(\%)$	Error $\Delta\omega_f$ (%)
	Flutter velocity U_f (m/s)	Critical frequency ω_f (rad/s)	Flutter velocity U_f (m/s)	Critical frequency ω_f (rad/s)		
2	99.30	1.682	98.74	1.708	-0.6	1.6
3	99.50	1.680	98.74	1.708	-0.8	1.7
4	99.60	1.679	98.93	1.706	-0.7	1.6
7	99.60	1.679	99.12	1.705	-0.5	1.5

Consequently, the multi-mode flutter analysis is also carried out on the combinations of fundamental mode shapes: first two, three, four and seven modes. The onset flutter results are presented in Table 2. It can be seen in the table that results obtained by the proposed method agree well with those derived from Ge and Tanaka (2000).

It is worth noting that the lumped formulation for the self-excited forces was employed in the approach proposed by Ge and Tanaka (2000). One reason for these differences between two solutions could be that by using difference of the self-excited forces formulation, the flutter velocity and critical velocity were discrepancies, and the comparison is only between the four mode combinations provided by both solutions but not considering size of the increment of reduced frequency ΔK.

Due to the target cantilevered structure under study, the first torsional mode is seen to coalesce with the first vertical bending mode, the empirical methods such as Selberg's (1961) and Rocard's (1963), and the classical thin airfoil methods of Kloppel (ECCS, 1987) and Put (1976) are employed for this case. For the comparison purpose, the results given by alternative multi-modes flutter analysis methods are also presented. Table 3 shows the comparison of the results of the flutter wind speeds and critical frequency with solutions derived from Kloppel and Thiele's approach (Ge and Tanaka, 2000).

Based on the proposed direct analysis, which considers all natural modes in the flutter analysis, the onset flutter of the

Table 3. Comparison of Flutter Analysis Results of the Cantilevered Thin Airfoil

Reference	Method	Flutter velocity U_f (m/s)	Critical frequency ω_f (rad/s)	Error $\Delta U_f(\%)$
Present	Direct	99.12	1.705	-1.5
	Two modes	98.74	1.708	-1.8
Simiu and Scanlan (1996)	Two modes	96.26	1.749	-4.3
Ge and Tanaka (2000)	Full-mode	99.80	1.678	-0.8
	Two modes	99.30	1.682	-1.3
Xie (Ge and Tanaka, 2000)	State-space	105.30	1.768	4.7
Cheng (Ge and Tanaka, 2000)	p-K-F	104.90	1.600	4.3
Rocard (1963)	Empiric	94.22	-	-6.3
Selberg (1961)	Empiric	93.88	-	-6.7
ECCS (1987)	Kloppel	100.60	-	-
Put (1976)	Put	107.30	-	6.7

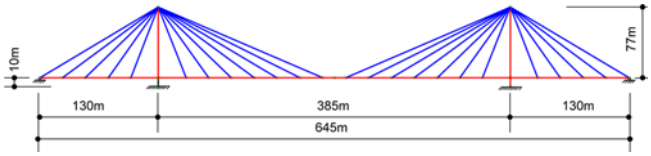

Fig. 5. Three-span Cable-stayed Bridge Model

cantilevered thin airfoil is estimated at the wind velocity of $U_f = 99.12(m/s)$, corresponding to the circle frequency $\omega_f = 1.705(rad/s)$. Table 3 reveals that results obtained by the proposed method are almost identical with the ones predicted by the other above-mentioned authors. It should be noted that the proposed methods, the direct analysis and the two modes are in good agreement with the exact analytical solution. The conclusion to be drawn from this analysis is that the combination of the first fundamental vertical bending and torsional modes is sufficient to correctly predict flutter onset of the cantilevered thin airfoil while any higher mode only makes little contribution to flutter onset.

4.1.2 Three-span Cable-stayed Bridge

The second validation considered here is the cable-stayed bridge that has a deck width, B of 18.0 m. The bridge has a 385.0 m center span between the pylons, and two 130.0 m anchor spans on each side of the pylon, the cross section of which is 18.0 m wide. The cables are arranged in a one-plane fan configuration with 24 cables as shown in Fig. 5. The finite element method idealizes this structure as a three-dimensional framework with 30 space beam elements and 24 space cable elements. The geometrical and structural properties of these elements were provided by Starossek (1991) as presented in Table 4. The value of the air density, ρ was adopted as 1.25 kg/m, and a constant modal damping ratio of critical $\xi = 0.3\%$ was assumed in this cable-stayed bridge.

A comparison of natural frequencies and mode shapes description for the first 6 modes is presented in Table 5. Furthermore, it is noted that the first fundamental symmetric vertical bending and torsion modes are the first and second modes, while the first fundamental asymmetric vertical bending and torsion modes are the third and fifth modes (Vu *et al.*, 2011b).

Based on the theoretical flutter derivatives, the proposed direct flutter method is conducted for the integrated wind-bridge system. Fig. 6 shows a diagram of the real part σ_j and the imaginary part ω_j versus the mean wind velocity, corresponding to the reduced frequency increment K_j for this analysis process.

Accordingly, two possible flutter states are found, and onset flutter values are calculated and compared with the results given by Starossek (1991) as gathered in Table 6. The effect of natural modes participating in the flutter instability was investigated by the multi-mode method.

Table 4. The Mechanical Properties of Three-span Cable-stayed Bridge

Mechanical properties	Deck	Tower	Cable
Area of cross section, A (m^2)	1.2	4.43	0.0125
Elastic modulus, E (Mpa)	210,000	210,000	200,000
Shear modulus, G (Mpa)	75,000	75,000	-
Lateral bending stiffness, EI_y (Mpam^4)	7,734,930	6,763,050	-
Vertical bending stiffness, EI_z (Mpam^4)	140,070	214,200	-
Torsional stiffness, GJ_x (Mpam^4)	22,950	750×10^9	-
Mass per unit length, m (kg/m)	0.0064	0.0063	-
Mass moment of inertia per unit length, I_m (kgm^2/m)	0.2000	0.0473	-

Table 5. Natural Frequencies and Mode Shapes of the Three-span Cable-stayed Bridge

Mode	Mode shape	Natural frequency, ω_f (rad/s)		Error $\Delta\omega$ (%)
		Starossek (1991)	Present	
1	V-S-1	2.468	2.471	0.1
2	T-S-1	2.764	2.768	0.1
3	V-A-1	3.533	3.663	3.7
4	V-S-2	5.241	5.252	0.2
5	T-A-1	5.528	5.566	0.7
6	V-A-2	5.998	6.207	3.5

Note: V = Vertical; T = Torsional; L = Lateral; S = Sysmetric; A = Asymetric

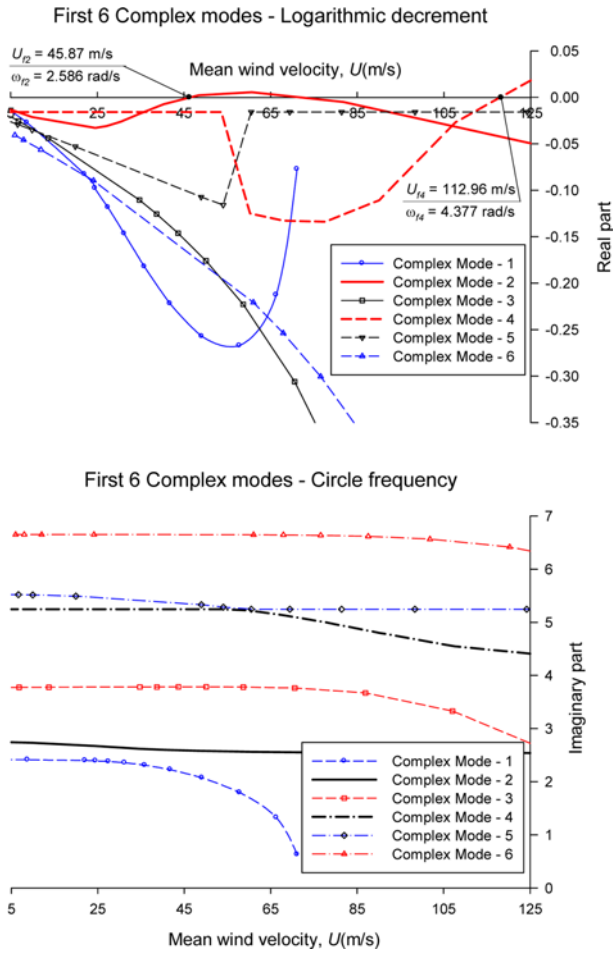

Fig. 6. Variation of Complex Eigenvalue for the Three-span Cable-stayed Bridge

Table 6. Results of Two Possible Critical Flutter States of the Three-span Cable-stayed Bridge

State	Mode	Flutter velocity U_f (m/s)		Critical frequency ω_f (rad/s)		Error ΔU_f(%)	Error $\Delta\omega_f$(%)
		Starossek (1991)	Present	Starossek (1991)	Present		
1	2	44.40	45.87	2.591	2.586	3.20	-0.18
2	4	112.00	112.96	4.377	4.487	0.85	2.45

Table 7. Comparison of Onset Flutter Results of the Three-span Cable-stayed Bridge

Reference	Method	Flutter velocity U_f (m/s)	Critical frequency ω_f (rad/s)	Error ΔU_f (%)	Error $\Delta\omega_f$(%)
Simiu and Scanlan (1996)	Two modes	42.84	2.615	-3.64	0.93
Starossek (1991)	Direct	44.40	2.591	-	-
Present	Direct	45.87	2.586	3.20	-0.18
	Two modes	49.90	2.578	11.01	-0.51

Table 7 shows the onset flutter results obtained by the proposed approach compared with those given by alternative methods. It can be seen that the bimodal flutter analysis methods Simiu and Scanlan (1996) that is based on the generalized 2-DOF model, leading to underestimation of the critical wind speed.

We note that Starossek (1991) employed the finite beam element which only regards to the vertical displacement (bending) and torsional displacement. Furthermore, the structural stiffness-proportional damping model is used in the structural flutter equation according to his method. The reasons for some discrepancies between results given in Tables 5, 6 and 7 obtained by the presented method with Starossek's results could be the difference of the used beam element in modeling the fluttering beam and difference of structural damping model.

However, it is clear that the present method shows reasonable results that are in good agreement with those of the reference method in all critical stages.

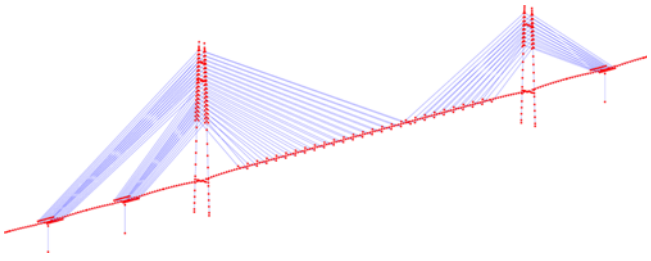

Fig. 7. Finite Element Model of the Asymmetric Bridge for Flutter Analysis

4.2 Flutter Analysis using the Experimental Flutter Derivatives

The last numerical example is to consider the New Millennium bridge, an asymmetric model of cable-stayed bridge with a main span of 510.0 m. The wind-tunnel tests of the section model and

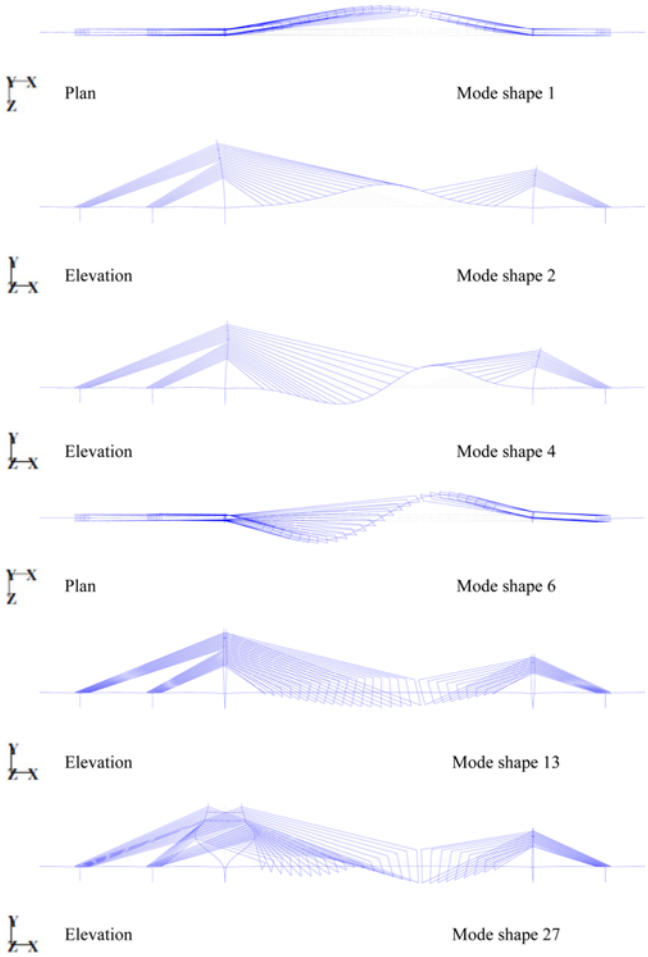

Fig. 9. Fundamental Mode Shapes of the Asymmetric Bridge

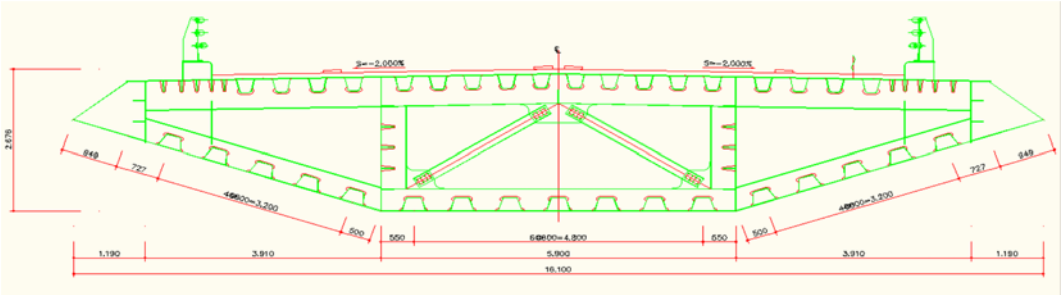

Fig. 8. Cross-section of Deck of the Asymmetric Bridge

full bridge model have been conducted by the Daewoo Institute of Construction Technology (DICT). A distinct feature of the bridge is its high (195.0 m) and low (135.0 m) pylons with two bundle cables in the rear span (Kim *et al.*, 2010). The structure is modeled by a three-dimensional framework with a total of 656 nodes, 772 elements (space beams, cables, and rigid links) and 279 nodal masses (Fig. 7). The space two-node catenary cable element is adopted, wherein both the 'self weight' and 'pretension' effects are taken into account in derivation of the stiffness matrix (Vu *et al.*, 2012). This element is good not only for simulating cables with small sags (i.e., large pretensions), but also cables with large sags (i.e., small pretensions). A constant modal damping ratio of critical $\zeta = 0.34\%$ is suggested for the section model tests. Fig. 8 shows that the bridge section has a streamlined steel box with a 16.1 m width and a 2.6 m height. For the free vibration analysis, some of the fundamental mode shapes of the cable-stayed bridge are presented in Fig. 9. The natural frequencies and mode shapes for the first 30 modes are shown in Table 8, which are essential for the analysis of the aerodynamic instability of the bridge under laminate wind flow approaches. It should be noted that the results computed by the present program are very close to those obtained by the program package MIDAS-Civil (MIDASIT, 2004). Full set of the flutter derivatives A_i^*, H_i^* and $P_i^*(i = \overline{1,6})$ are shown in Fig. 10.

Based on the proposed multi-mode flutter algorithm, the coupled flutter problem of the asymmetric bridge is analyzed by performing a series of complex-eigen analyses. According to the

Table 8. Comparison of Natural Frequencies and Mode Shapes of the Asymmetric Bridge

Mode No.	Natural frequency, ω_f (*rad/s*)			Mode shape
	MIDAS (2004)	Present	Error (%)	
1	1.650	1.677	-1.65	L-S-1
2	1.968	1.975	-0.35	V-S-1
3	2.682	2.849	-2.40	HP-L-A-1
4	2.845	2.876	-1.08	V-A-1
5	3.723	3.728	-0.14	V-S-2
6	4.105	4.181	-1.85	L-A-1
7	4.468	4.664	-4.38	LP-L-A-1
8	4.651	4.790	-2.99	V-A-2
9	5.434	5.458	-0.44	V-A-3
10	5.735	5.929	-3.38	LS-L-S-1
11	6.041	6.060	-0.32	V-S-3
12	6.987	6.963	0.33	V-A-4
13	7.112	7.071	0.57	T-S-1
14	7.184	7.184	0.00	V-A-5
15	7.506	7.388	1.56	T-S-2
16	7.512	7.499	0.17	V-A-6
17	8.299	8.080	2.64	V-S-4
18	8.563	8.551	0.14	SS-V-S-1
19	8.709	8.930	-2.54	SS-L-S-1
20	9.071	9.092	-0.23	V-S-5
21	9.577	9.585	-0.08	LS-V-S-1
22	9.701	10.145	-4.59	LS-L-A-2
23	10.117	10.196	-0.79	HP-L-A-2
24	10.986	11.045	-0.54	L-A-2
25	11.016	11.348	-3.02	V-A-7
26	11.106	11.670	-4.14	HP-L-S-1
27	11.983	12.776	1.59	T-A-1
28	13.246	13.172	0.56	T-A-2
29	13.475	13.448	0.20	V-S-6
30	14.571	14.102	3.22	V-A-8

Note: V = Vertical; T = Torsional; L = Lateral; S = Sysmetric; A = Asymmetric; HP = High Pylon; LP = Low Pylon; SS = Small Side span; LS = Large Side span.

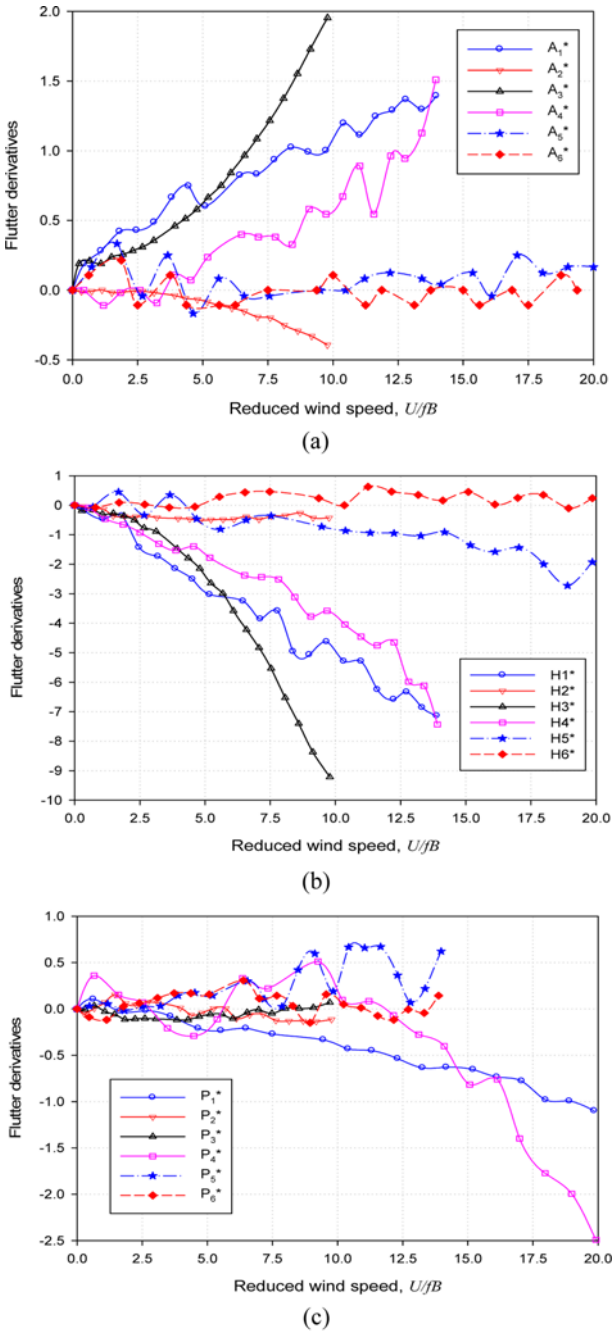

Fig. 10. Flutter Derivatives for the Asymmetric Bridge: $A_i^*(i = \overline{1,6})$ (b) $H_i^*(i = \overline{1,6})$ (c) $P_i^*(i = \overline{1,6})$

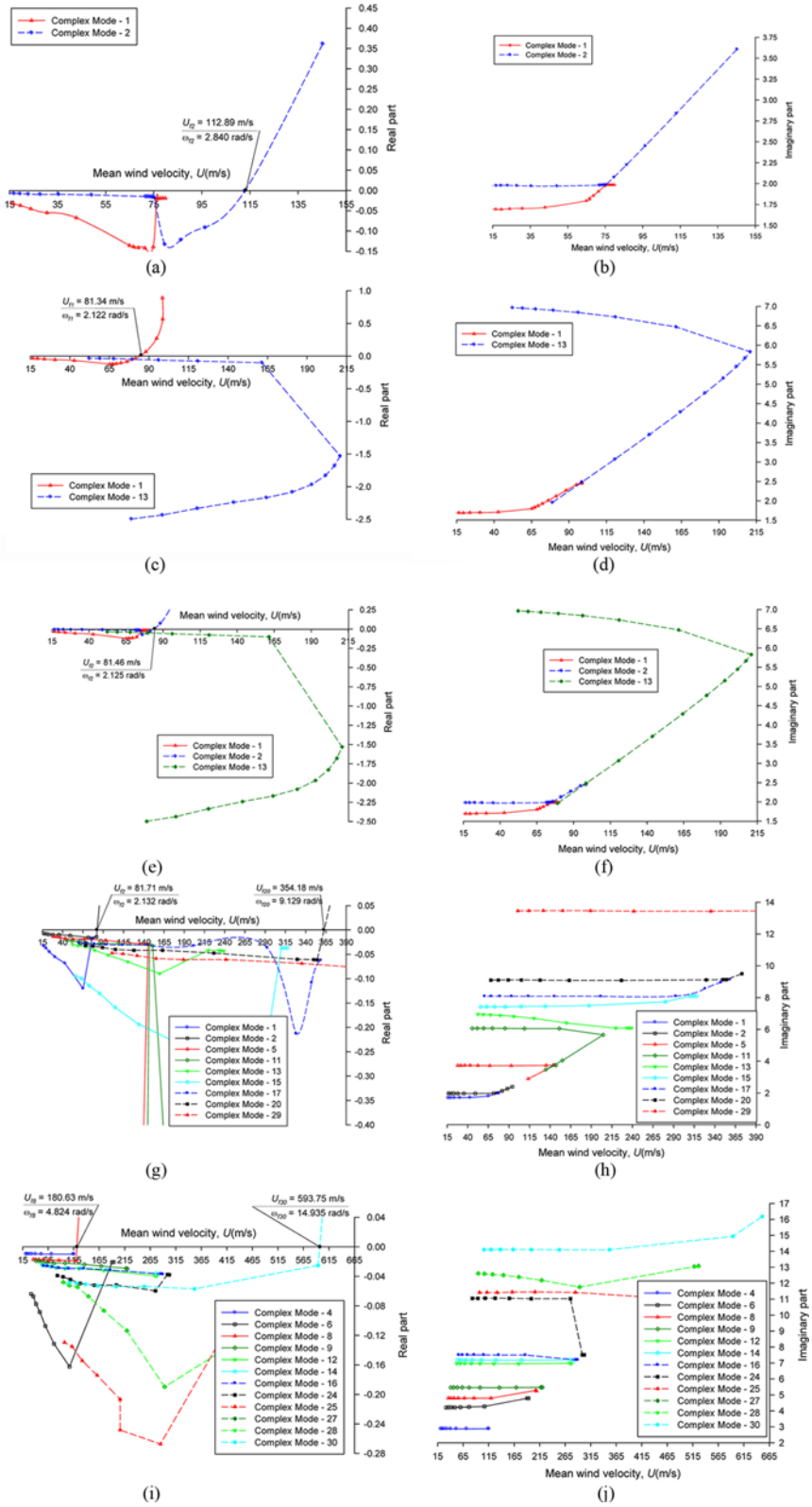

Fig. 11. Flutter Eigenvalue Evolution of the Asymmetric Bridge: (a) First 2 Modes (1st Lateral, Vertical mode) - Logarithmic Decrement, (b) First 2 Modes (1st Lateral, Vertical mode) - Circle Frequency, (c) Fundamental Modes (1st Lateral, Torsional mode) - Logarithmic Decrement, (d) Fundamental Modes (1st Lateral, Torsional mode) - Circle frequency, (e) Fundamental Modes (1st Lateral, Vertical,Torsional mode) - Logarithmic Decrement, (f) Fundamental Modes (1st Lateral, Vertical,Torsional mode) - Circle frequency, (g) Sysmetrical Modes - Logarithmic Decrement, (h) Sysmetrical Modes - Circle Frequency, (i) Asysmetrical Modes - Logarithmic Decrement, (j) Asysmetrical Modes - Circle Frequency

Table 9. Flutter Analysis Results by Using Contributed Modes for the Asymmetric Bridge

References	Contributed modes	Error U_f (%)	Flutter velocity U_f (m/s)	Critical frequency ω_f (rad/s)
Ding *et al*. (2002)	First 30 modes	-6.80	78.29	2.042
Present	First 2 modes (1,2)	34.39	112.89	2.840
	Fundamental modes (1,13)	-3.17	81.34	2.122
	Fundamental modes (1,2,13)	-3.02	81.46	2.125
	Symmetrical modes (1,2,5,11,13,15,17,20,29)	-3.04	81.71	2.132
	Asymmetrical modes (4,6,8,9,12,14,16,24,25,27,28,30)	115.03	180.63	4.824
	First 30 modes	-2.74	81.70	2.131
Experiment (Kim *et al*., 2002)	-	-	84.0	-

results, multiple intersection points may occur, showing the theoretical instability at a certain reduction of frequency. Thus, the critical wind velocity for flutter should be a minimum value corresponding to its frequency. Five fundamental combinations are adopted for flutter analysis.

First, by regarding the first 2 modes that were of first symmetric vertical and lateral bending, the evolution of the real and imaginary parts of the complex eigen-value is depicted in Fig. 11(a). With this combination, the flutter wind speed of U_{f2} = 112.89 m/s and critical frequency of ω_{f2} = 2.840 rad/s were concurrently obtained. Next, by including the first symmetric lateral bending and first symmetric torsion modes, the results of the complex eigenvalue analysis are illustrated in Fig. 11(b), and the onset flutter is at U_{f1} = 81.34 m/s and ω_{f1} = 2.122 rad/s. It should be noted that a combination of first symmetric vertical bending and symmetric torsion mode could not provide a possible critical flutter state for this bridge case. The combination of the first 3 modes consists of the first symmetric vertical, lateral and torsional modes leading to flutter estimation at U_{f2} = 81.46 m/s and ω_{f2} = 2.125 rad/s as shown in Fig. 11(c). Then, the addition of symmetrical modes is comprised in the first 30 modes. An evolution diagram is illustrated in Fig. 11(d). It is observed that two possible critical flutter states are found; however, the onset flutter was estimated at U_{f2} = 81.71 m/s and ω_{f2} = 2.132 rad/s. For the case of the asymmetric bridge, a combination of asymmetrical modes is examined for possible onset flutter. The evolution diagram of this case is shown in Fig. 11(e), wherein the flutter prediction is at U_{f3} = 180.63 m/s and ω_{f3} = 4.824 rad/s.

Table 9 shows a comparison of the flutter wind velocity and the critical frequency predicted by the present method, the Ding *et al*. (2002) method, and the aeroelastic full model test for the bridge in service stage (Kim *et al.*, 2010). Comparing the first 2 modes, the combination of fundamental modes of the modes 1, 13 or modes 1, 2, 13 with the first 30 modes results, the contribution of the first symmetric vertical bending mode may not affect the critical flutter velocity; meanwhile, the first symmetric lateral bending mode plays an important role in generating the coupled flutter. In a similar comparison, a combination of the asymmetric modes leads to an overestimation in the results of the onset flutter, while a combination of the symmetric modes permits the accurate prediction of flutter wind speed and critical frequency results. The use of the proposed multi-mode flutter analysis procedure predicts the flutter speed of 81.70 m/s and critical frequency of 2.131 rad/s, which are in good agreement with those obtained by the Ding *et al.* (2002) method and the value of flutter speed is also very close to the experimental result.

We may see that both the structural mass and the self-excited forces model based on the consistent form were employed in the present method, while Ding *et al*. (2002) utilized the lumped form model. It is leading to numerical discrepancies in the both methods' results, although these methods employed the same size of the increment of the reduced frequency ΔK.

Comparison in the critical wind speeds indicating that the lumped form model of aerodynamic forces provides conservative result, meaning the predicted flutter speed value is lower than those obtained by the present method and measured from the wind tunnel.

5. Conclusions

This paper presents the convenient finite element-based method employing the consistent self-excited aerodynamic force formulations with eighteen flutter derivatives utilized by complex notation for the coupled flutter analysis of long-span bridges. The flutter onset predictions are compared with those either given by existing methods or the wind tunnel test discussed through numerical examples showing the effectiveness and accuracy of the present approach.

The coupled flutter problem of the asymmetric bridge with considering full set of flutter derivatives is analyzed as one of applications for engineering practice. Numerical analysis results indicate that two fundamental modes; first symmetric lateral and torsional, are played the significant roles in generating the bridge flutter. Multi-mode analyses that are based on only the symmetrical modes can predict accurately the bridge flutter onset.The traditional combination of first symmetric vertical bending and symmetric torsion mode, which are often employed in the bimodal coupled flutter analysis, cannot be used to predict the onset flutter for this asymmetric bridge. The consistent self-excited aerodynamic force formulations produce the flutter velocity that is closer to the experimental one of full-bridge model in the wind tunnel.

Acknowledgements

The financial support for the present research work by the Ministry of Land, Transport and Maritime Affairs of Korean Government through Super Long Span Bridge R&D Center is gratefully acknowledged.

References

Agar, T. T. A. (1989). "Aerodynamic flutter analysis of suspension bridges by a modal technique." *Eng. Struct*., Vol. 11, No. 2, pp. 75-82, DOI: 10.1016/0141-0296(89)90016-3.

Arnoldi, W. E. (1951). "The principle of minimised iterations in the solutions of the matrix eigenvalue problem." *Quart. Appl. Math.*, Vol. 9, No. 17, pp. 17-29.

Bartoli, G. and Mannini, C. (2008). "A simplified approach to bridge deck flutter." *J. Wind Eng. Ind. Aerodyn.*, Vol. 96, No. 2, pp. 229-256, DOI: 10.1016/j.jweia.2007.06.001.

Bleich, F. (1949). Dynamic instability of truss-stiffened suspension bridges under wind action." *Trans. Am. Soc. Civ. Eng.*, Vol. 114, No. 1, pp. 1177-1222.

Chen, X., Matsumoto, M., and Kareem, A. (2000). "Aerodynamic coupling effects on flutter and buffeting of bridges." *ASCE J. Eng. Mech*., Vol. 126, No. 1, pp. 17-26, DOI: 10.1061/(ASCE)0733-9399(2000) 126:1(17).

Chen, X. and Kareem, A. (2006). "Revisiting multimode coupled bridge flutter: Some new insights." *J. Eng. Mech.*, Vol. 132, No. 10, pp. 1115-1116, DOI: 10.1061/(ASCE)0733-9399(2006)132:10(1115).

Chen, X. and Kareem, A. (2007). "Improved understanding of bimodal coupled bridge flutter based on closed-form solutions." *J. Struct. Eng*., Vol. 133, No. 1, pp. 22-31, DOI: 10.1061/(ASCE)0733-9445 (2007)133:1(22).

Clough, R. W. and Penzien, J. (1993). *Dynamics of structures*, 2nd Edition, McGraw-Hill, New York.

Ding, Q. S., Chen, A. R., and Xiang, H. F. (2002). "Coupled flutter analysis of long-span bridges by multimode and full-order approaches." *J. Wind Eng. Ind. Aerodyn*., Vol. 90, Nos. 12-15, pp. 1981-1993, DOI: 10.1016/S0167-6105(02)00315-X.

Dung, N. N., Miyata, T., Yamada, H., and Minh, N. N. (1998). "Flutter responses in long span bridges with wind induced displacement by the mode tracing method." *J. Wind Eng. Ind. Aerodyn*, Vols. 77-78, No. 1, pp. 367-379, DOI: 10.1016/S0167-6105(98)00157-3.

ECCS (1987). *Recommendations for calculating the effects of wind on constructions*, 2nd Edition, Technical Committee 12, Brussels, Belgium.

Ge, Y. J. and Tanaka, H. (2000). "Aerodynamic analysis of cable-supported bridge by multi-mode and full-mode approaches." *J. Wind Eng. Ind. Aerodyn.*, Vol. 86, Nos. 2-3, pp. 123-153, DOI: 10.1016/S0167-6105(00) 00007-6.

Jain, A., Jones, N. P., and Scanlan, R. H. (1996). "Coupled aeroelastic and aerodynamic response analysis of long-span bridges." *J. Wind Eng. Ind. Aerodyn*., Vol. 60, No. 1, pp. 69-80, DOI: 10.1016/0167-6105(96)00024-4.

Katsuchi, H., Jones, N. P., and Scanlan, R. H. (1999). "Multimode coupled flutter and buffeting analysis of the Akashi-Kaikyo Bridge." *ASCE J. Struct. Eng*., Vol. 125, No. 1, pp. 60-70, DOI: 10.1061/(ASCE)0733-9445(1999)125:1(60).

Kim, D. Y., Kim, H. Y., Kim, Y. M., Kwak, Y. H., Park, J. G., and Shin, S. H. (2010). *Wind engineering studies for the New Millennium Bridge (1st Site)*, Technical Report, DAEWOO Institute of Construction Technology.

Lee, H. E., Vu, T. V., Yoo, S. Y., and Lee, H. Y. (2011). "A simplified evaluation in critical frequency and wind speed to bridge deck flutter." *Procedia Engineering*, Vol. 14, No. 1, pp. 1784-1790, DOI: 10.1016/j.proeng.2011.07.224.

Matsumoto, M. (1999). "Recent study on bluff body aerodynamics and its mechanism." *Proc. 10th Int. Conf. on Wind Eng.*, Copenhagen, Denmark, pp. 67-78.

MIDASIT, MIDAS gen analysis & design manual (2004). MIDAS Information Technology Cooperation.

Mishra, S. S., Kumar, K., and Krishna, P. (2008). "Relevance of eighteen flutter derivatives in wind response of a long-span cable-stayed bridge." *ASCE J. Struct Eng*., Vol. 134, No. 5, pp. 769-781, DOI: 10.1061/(ASCE)0733-9445(2008)134:5(769).

Namini, A., Albrecht, P., and Bosch, H. (1992). "Finite element-based flutter analysis of cable-suspended bridges." *ASCE J. Struct. Eng.*, Vol. 118, No. 6, pp. 1509-1526, DOI: 10.1061/(ASCE)0733-9445 (1992)118:6(1509).

Put, V. D. (1976). "Rigidity of structures against aerodynamic forces." *Int. Ass. of Bridge and Struct. Eng*., Vol. 36, No. 1, pp. 189-196, DOI: 10.5169/seals-917.

Rocard, Y. (1963). *Instabilite des Ponts Suspendus dans le Vent-Experiences sur Modele Reduit*, Nat. Phys. Lab., Paper 10.

Sarkar, P. P., Jones, N. P., and Scanlan, R. H. (1994). "Identification of aeroelastic parameters of flexible bridges." *ASCE J. Eng. Mech*., Vol. 120, No. 8, pp. 1718-1742, DOI: 10.1061/(ASCE)0733-9399 (1994) 120:8(1718).

Scanlan, R. H. and Tomko, J. J. (1971). "Airfoil and bridge deck flutter derivatives." *ASCE J. Eng. Mech. Div*., Vol. 97, No. 6, pp. 1117-1137.

Scanlan, R. H. (1978). "Action of flexible bridges under wind, 1: flutter theory." *J. Sound Vib*., Vol. 60, No. 2, pp. 187-199, DOI: 10.1016/S0022-460X(78)80028-5.

Selberg, A. (1961). "Oscillation and aerodynamic stability of suspension bridges." *Acta. Polytech. Scand*., Vol. 13, No. 1, pp. 308-377.

Simiu, E. and Scanlan, R. H. (1996). *Wind Effects on Structures: Fundamentals and Applications to Design*, 3rd Edition, Wiley, New York.

Starossek, U. (1991). *Bruckendynamik-Winderregte Schwingungen von Seibrucken*, PhD Thesis, University of Stuttgart, Vieweg & Sohn Verlags-GmbH, Braunschweig, Germany, (in German).

Starossek, U. (1998). "Complex notation in flutter analysis." *ASCE J. Struct. Eng*., Vol. 124, No. 8, pp. 975-977, DOI: 10.1061/(ASCE) 0733-9445(1998)124:8(975).

Tanaka, H., Yamamura, N., and Tatsumi, M. (1992). "Coupled mode flutter analysis using flutter derivatives." *J. Wind Eng. Ind. Aerodyn*., Vol. 42, Nos. 1-3, pp. 1279-1290, DOI: 10.1016/0167-6105(92)90135-W.

Theodorsen, T. (1935). *General theory of aerodynamic instability and the mechanism of flutter*, NACA Report No. 496.

Vu, T. V. (2010). *Aeroelastic flutter analysis of long-span bridges*, Ph.D Thesis, Korea University, South Korea.

Vu, T. V., Kim, Y. M., Han, T. S., and Lee, H. E. (2011a). "Simplified formulations for flutter instability analysis of bridge deck." *J. Wind & Structures*, Vol. 14, No. 4, pp. 359-381, DOI: 10.12989/was.2011.14.4.359.

Vu, T. V., Kim, Y. M., Lee, H. Y., Yoo S. Y., and Lee, H. E. (2011b). "Flutter analysis of bridges through use of by state space method." *Proc. 8th Int. Conf. Struct. Dyn., EURODYN 2011*, Belgium,Vol. 1, pp. 3083-3090.

Vu, T. V., Lee, H. E., and Bui, Q. T. (2012). "Nonlinear analysis of cable-supported structures with a spatial catenary cable element." *J. Struct. Eng. & Mechanics*, Vol. 43, No. 5, pp. 583-605, DOI: 10.12989/sem.2012.43.5.583.

Vu, T. V., Lee, H. Y., Choi, B. H., and Lee, H. E. (2013). "Prediction of bridge flutter under a crosswind flow." *J. Wind & Structures*, Vol. 17, No. 3, pp. 275-298, DOI: 10.12989/was.2013.17.3.275.

Weaver, W. Jr. and Johnston, P. R. (1987). *Structural dynamics by finite elements*, Prentice-Hall, Englewood Cliffs, NJ.

Zhang, X. J., Xiang, H. F., and Sun, B. N. (2002). "Nonlinear aerostatic and aerodynamic analysis of long-span suspension bridges considering wind-structure interaction." *J. Wind Eng. Ind. Aerodyn.*, Vol. 90, No. 9, pp. 1065-1080, DOI: 10.1016/S0167-6105(02)00251-9.

Zhang, X. and Brownjohn, J. M. W. (2005). "Some considerations on the effects of the P-derivatives on bridge deck flutter." *J. Sound and Vibration*, Vol. 283, Nos. 3-5, pp. 957-969, DOI: 10.1016/j.jsv.2004.05.031.

Appendix.

Consistent aerodynamic element matrix including the 18 flutter derivatives.

Assuming that the length of the element is sufficiently small, the flutter derivatives and mean wind speed approach to the element can be regarded as a uniform distribution with respect to its axis local coordinate. Hence, the integration calculation could be solved over its length. Conforming with the structural property matrices (stiffness and mass), assuming that the aerodynamic matrix has a of square matrix of order 12, it is divided into sub-matrices:

$$[A_{ae}^{e}] = \begin{bmatrix} a^{uu} & a^{u\alpha} & a^{uh} & a^{up} \\ a^{\alpha u} & a^{\alpha\alpha} & a^{\alpha h} & a^{\alpha p} \\ a^{hu} & a^{h\alpha} & a^{hh} & a^{hp} \\ a^{pu} & a^{p\alpha} & a^{ph} & a^{pp} \end{bmatrix} \tag{22}$$

It is found that the nonzero-coefficients of matrix [$\mathbf{A}_{ae}$] are given by,

$$a^{\alpha\alpha} = \pi\rho b^4 \int_0^L C_{M\alpha}\{N_1\}\{N_1\}^T dx \tag{23}$$

$$a^{\alpha h} = \pi\rho b^3 \int_0^L C_{Mh}\{N_1\}\{N_2\}^T dx \tag{24}$$

$$a^{\alpha p} = \pi\rho b^3 \int_0^L C_{Mp}\{N_1\}\{N_2\}^T dx \tag{25}$$

$$a^{h\alpha} = \pi\rho b^3 \int_0^L C_{L\alpha}\{N_2\}\{N_1\}^T dx \tag{26}$$

$$a^{hh} = \pi\rho b^4 \int_0^L C_{Lh}\{N_2\}\{N_2\}^T dx \tag{27}$$

$$a^{hp} = \pi\rho b^2 \int_0^L C_{Lp}\{N_2\}\{N_2\}^T dx \tag{28}$$

$$a^{p\alpha} = \pi\rho b^3 \int_0^L C_{D\alpha}\{N_2\}\{N_1\}^T dx \tag{29}$$

$$a^{ph} = \pi\rho b^2 \int_0^L C_{Dh}\{N_2\}\{N_2\}^T dx \tag{30}$$

$$a^{pp} = \pi\rho b^4 \int_0^L C_{Dp}\{N_2\}\{N_2\}^T dx \tag{31}$$

and the sub-matrices of a^{uu}, $a^{u\alpha}$, a^{uh}, a^{up}, $a^{\alpha u}$, a^{hu}, a^{pu} have zero coefficients. Evaluation of the above integrals leads to:

$$a^{\alpha\alpha} = \pi\rho b^4 C_{M\alpha}\frac{L}{6}\begin{bmatrix} 2 & 1 \\ 1 & 2 \end{bmatrix} \tag{32}$$

$$a^{\alpha h} = \pi\rho b^4 C_{Mh}\frac{L}{60}\begin{bmatrix} 21 & 9 & 3L & -2L \\ 9 & 21 & 2L & -3L \end{bmatrix} \tag{33}$$

$$a^{\alpha p} = \pi\rho b^3 C_{Mp}\frac{L}{60}\begin{bmatrix} 21 & 9 & 3L & -2L \\ 9 & 21 & 2L & -3L \end{bmatrix} \tag{34}$$

$$a^{h\alpha} = \pi\rho b^3 C_{L\alpha}\frac{L}{6}\begin{bmatrix} 21 & 9 \\ 9 & 21 \\ 3L & 2L \\ -2L & -3L \end{bmatrix} \tag{35}$$

$$a^{hh} = \pi\rho b^2 C_{Lh}\frac{L}{420}\begin{bmatrix} 156 & 54 & 22L & -13L \\ 54 & 156 & 13L & -22L \\ 22L & 13L & 4L^2 & -3L^2 \\ -13L & -22L & -3L^2 & 4L^2 \end{bmatrix} \tag{36}$$

$$a^{hp} = \pi\rho b^2 C_{Lp}\frac{L}{420}\begin{bmatrix} 156 & 54 & 22L & -13L \\ 54 & 156 & 13L & -22L \\ 22L & 13L & 4L^2 & -3L^2 \\ -13L & -22L & -3L^2 & 4L^2 \end{bmatrix} \tag{37}$$

$$a^{p\alpha} = \pi\rho b^3 C_{D\alpha}\frac{L}{60}\begin{bmatrix} 21 & 9 \\ 9 & 21 \\ 3L & 2L \\ -2L & -3L \end{bmatrix} \tag{38}$$

$$a^{ph} = \pi\rho b^2 C_{Dh}\frac{L}{420}\begin{bmatrix} 156 & 54 & 22L & -13L \\ 54 & 156 & 13L & -22L \\ 22L & 13L & 4L^2 & -3L^2 \\ -13L & -22L & -3L^2 & 4L^2 \end{bmatrix} \tag{39}$$

$$a^{pp} = \pi\rho b^2 C_{Dp}\frac{L}{420}\begin{bmatrix} 156 & 54 & 22L & -13L \\ 54 & 156 & 13L & -22L \\ 22L & 13L & 4L^2 & -3L^2 \\ -13L & -22L & -3L^2 & 4L^2 \end{bmatrix} \tag{40}$$